

Requirements for very high temperature Kohn-Sham DFT simulations and how to bypass them

A. Blanchet,^{1,2, a)} M. Torrent,^{1,2} and J. Clérouin^{1,2,3}

¹⁾CEA-DAM-DIF, F-91297 Arpajon, France

²⁾Université Paris-Saclay, CEA, Laboratoire Matière sous conditions extrêmes, 91680 Bruyères-le-Châtel, France

³⁾Corresponding author^{b)}

(Dated: 19 November 2020)

In high temperature density functional theory simulations (from tens of eV to keV) the total number of Kohn-Sham orbitals is a critical quantity to get accurate results. To establish the relationship between the number of orbitals and the level of occupation of the highest energy orbital, we derived a model based on the homogeneous electron gas properties at finite temperature. This model predicts the total number of orbitals required to reach a given level of occupation and thus a stipulated precision. Levels of occupation as low as 10^{-4} , and below, must be considered to get converged results better than 1%, making high temperature simulations very time consuming beyond a few tens of eV. After assessing the predictions of the model against previous results and ABINIT minimizations, we show how the extended FPMD method of Zhang *et al.* [PoP **23** 042707, 2016] allows to bypass these strong constraints on the number of orbitals at high temperature.

I. INTRODUCTION

Kohn-Sham density functional theory (KSDFT^{1,2}) simulations are now a well-established technique to compute static and dynamical properties of matter at ambient conditions, and are implemented in simulation packages such as VASP³, QUANTUM ESPRESSO⁴ or ABINIT⁵⁻⁷. The extension of this technique towards hot systems was historically introduced in VASP, through the Mermin finite temperature functional⁸, where orbitals are populated according to the Fermi-Dirac statistics. This approach, well adapted up to a few eV, which corresponds to the domain of liquid metals⁹, becomes more expensive at higher temperatures (tens of eV), entering the warm dense matter regime (WDM). More precisely, the shape of the Fermi-Dirac distribution, strongly depends on the ratio θ of the temperature to the Fermi temperature. The latter scales as $n_e^{2/3}$, where n_e is the electronic density (see Eq. 2). For materials at standard density, θ quickly becomes higher than one as the temperature rises, flattening the Fermi distribution. This flattening is responsible for the large number of orbitals to be included in the simulations. Conversely, for strongly compressed materials, θ remains lower than one (degenerate matter), even at high temperatures. The Fermi-Dirac distribution stays close to its zero temperature shape, allowing for KSDFT simulations of compressed materials at high temperatures¹⁰⁻¹⁵ with a small number of orbitals.

To avoid this difficulty, techniques taking advantage of the principle of the *nearsightedness* of the one particle density matrix, introduced by Kohn^{16,17}, have been developed. Among them, the path-integral Monte-Carlo (PIMC) method in the restricted path approximation, is now able to treat elements of the second row of the periodic table¹⁸⁻²⁰. Other methods based on the density matrix are also explored (spectral quadrature²¹, stochastic²², mixed²³), and are increasingly

faster with increasing temperature, scaling linearly with the size of the system. But these approaches are computationally very demanding, especially at low temperature, with the exception of the mixed method which takes advantage of both representations (orbitals and density matrix). Another alternative, much less time consuming, is provided by average atom models, that solve the Schrödinger or the Dirac equations in a box, coupled or not with a structural evaluation through the resolution of integral equations such as hyper-netted-chain (HNC). One can mention Purgatorio²⁴, the pseudo-atom molecular dynamics model^{25,26}, the neutral pseudo-atom model²⁷ or the SCAALP model^{28,29}.

For the dense plasma regime, a simplified approach has been proposed, using an orbital-free (OFDFT) formulation of the electronic kinetic energy based on the finite temperature Thomas-Fermi theory and its extensions^{30,31}. This method, well adapted for dense plasmas simulations and their mixtures³²⁻³⁴, is very fast for temperatures beyond tens of eV, but yields poor results below. To ensure accurate results at low temperature with the OFDFT approach, and, in particular, a satisfying description of chemical bonds, more elaborated functionals and a better treatment of exchange-correlation must be included³⁵⁻³⁹. The transition from the KSDFT formulation at low temperature to the OFDFT, as the temperature rises, is described in^{40,41}, and solutions have been proposed using the bootstrap method⁴² to compute Hugoniot or by introducing a KSDFT reference points⁴³ to build a coherent equation of state.

More recently, Zhang *et al.*⁴⁴ proposed to extend the KS-DFT approach at high temperature by replacing high energy orbitals by plane waves. Introducing the homogeneous electron gas (HEG) properties at high energy, the so-called extended FPMD method makes the connection with OFDFT approaches at high temperature but preserves the KS orbitals at low temperature. By keeping a minimum number of orbitals as the temperature rises, this method allows for a continuous transition from cold materials to hot plasmas.

A systematic comparison of the different approaches mentioned above was the subject of two blind comparison work-

^{a)}email address: augustin.blanchet@cea.fr

^{b)}email address: jean.clerouin@cea.fr

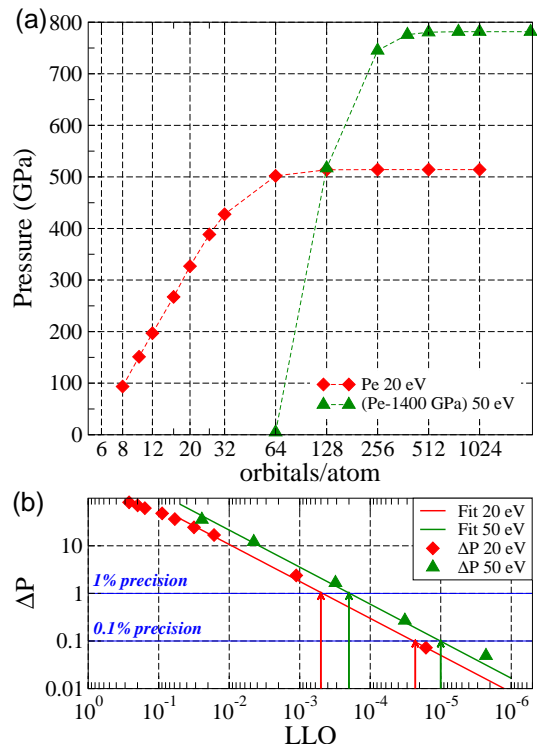


FIG. 1. (Color online) (a) Convergence of the electronic pressure versus the number of orbitals per atom for a 4 aluminum atoms at standard density ρ_0 and at 20 (red diamonds) and 50 eV (green triangles). For 50 eV pressures are shifted down by 1400 GPa. (b) Relative accuracy, in percentage, of the pressure calculation $\Delta P = 100|P - P_0|/P_0$ versus LLO, where P_0 is the pressure given by the highest number of orbitals (see Tables I and II). Red diamonds are for 20 eV data, and green up triangles for 50 eV. Corresponding straight lines are least squares fits and the horizontal blue lines the 1% and 0.1 % precision. Red and green arrows indicate the LLO required for 1% (resp. 0.1 %) precision at 20 and 50 eV. Note that the abscissa scale is reversed. Data with a LLO smaller than 10^{-6} are not represented.

shops, one on the equations of state⁴⁵ and the other on transport coefficients⁴⁶.

In this paper we provide quantitative prescriptions for high temperature KSDFT simulations. After discussing an example illustrating the convergence of the pressure with the number of orbitals involved in the calculation, we introduce a simple model based on the homogeneous electron gas to predict the number of orbitals required to reach a stipulated occupancy. We then compare these predictions with ABINIT minimizations and with previous molecular dynamics simulations at high temperature^{10,36,47}. To bypass these convergence constraints, we discuss the recently introduced extended FPMD method. We show, through its implementation in the ABINIT software package, how very high temperature (2000 eV) simulations are easily performed with the same level of accuracy as PIMC calculations despite a low number of orbitals.

TABLE I. Finite temperature evaluation of the electronic pressure of four aluminum atom at standard density and 20 eV for a varying number of orbitals. The PAW pseudo-potential involves 11 electrons. The horizontal line between 64 and 128 orbitals delimits the 1% precision region.

Orbitals /atom	LLO	Pressure GPa	ΔP %
8	$2.6 \cdot 10^{-1}$	93.49901	82
10	$2.0 \cdot 10^{-1}$	151.10035	71
12	$1.6 \cdot 10^{-1}$	196.87071	62
16	$8.9 \cdot 10^{-2}$	267.26940	48
20	$5.9 \cdot 10^{-2}$	326.88243	36
26	$3.2 \cdot 10^{-2}$	388.38812	24
32	$1.6 \cdot 10^{-2}$	427.61530	17
64	$1.1 \cdot 10^{-3}$	501.95302	2.4
128	$1.6 \cdot 10^{-5}$	513.83618	0.07
256	$2.0 \cdot 10^{-8}$	514.20696	0.0002
512	$3.5 \cdot 10^{-13}$	514.20793	0.
1024	$1.0 \cdot 10^{-15}$	514.20793	0.

TABLE II. Same as Table I at 50 eV. The horizontal line between 256 and 384 orbitals delimits the 1% precision region.

Orbitals /atom	LLO	Pressure GPa	ΔP %
64	$2.4 \cdot 10^{-2}$	1404.858	35
128	$4.5 \cdot 10^{-3}$	1917.023	12
256	$3.1 \cdot 10^{-4}$	2145.269	1.7
384	$3.2 \cdot 10^{-5}$	2175.835	0.27
512	$2.3 \cdot 10^{-6}$	2180.651	0.04
768	$1.3 \cdot 10^{-7}$	2181.678	0.0017
1024	$5.4 \cdot 10^{-9}$	2181.722	0.00027
2048	$< 10^{-18}$	2181.716	0.

II. CONVERGENCE WITH THE NUMBER OF ORBITALS

We show in Fig. 1 (a) the electronic pressure of aluminum at standard density and a temperature of 20 eV and 50 eV (shifted down by 1400 GPa), computed as a function of the number of orbitals. We define the convergence by the relative error, in percentage, of the electronic pressure $\Delta P = 100|P - P_0|/P_0$, where P_0 is the pressure obtained with the largest number of orbitals. One can see that 128 orbitals per atom are needed at 20 eV, and 384 at 50 eV to reach a convergence better than 1% (see numbers in Tables I and II). Let us recall that at low temperature, for 11 valence electrons, six doubly occupied orbitals⁴⁸, are sufficient. The increase from 6 to 128 orbitals per atom represents a computational effort for KSDFT calculations about 20^3 higher (35^3 at 50 eV). At high temperature we encounter a paradox situation where a large number of quasi-empty orbitals must be included with a computational cost proportional to the cube of this number (orthogonalization constraint). Detailed estimations of the number of orbitals required for a stipulated precision can be found in recent papers^{36,47,49,50}, upon which we will assess

our analysis.

The accuracy of the pressure estimation depends on the number of orbitals, because, as soon as the electronic temperature is non-zero, the distribution of the electronic orbitals is no longer bounded and goes *stricto sensu* to infinity. In simulations, involving a finite number of orbitals, the last orbital in energy has a certain level of occupancy, that we will call the last level occupancy (LLO). The first condition for doing sound simulations is to ensure that the LLO is low enough to give converged quantities. As shown in a recent study of MgO in the warm dense regime¹⁵, a LLO of 10^{-5} is necessary to obtain a better than 0.1% converged pressure above 100 eV. The convergence ΔP versus LLO is reported in Fig. 1 (b) and in Tables I and II for 20 and 50 eV. Data with a LLO smaller than 10^{-6} are not represented. The low LLO side of Fig. 1 (b), beyond 10^{-2} clearly exhibits a power law. An empirical relation between the relative error in the pressure ΔP and the LLO α is $\Delta P = a\alpha^b$, with $a = 382$ and $b = 0.78$ for 20 eV (Fig. 1 (b), solid red line), and $a = 769$, $b = 0.78$ for 50 eV (Fig. 1 (b), solid green line). These empirical scalings, that seem weakly dependent on the temperature, give a good order of magnitude of the last level occupation α required for a precision ΔP

$$\alpha = \left(\frac{\Delta P}{a} \right)^{1/b}. \quad (1)$$

In particular, to get a precision of 1% (resp. 0.1%), a LLO of $5 \cdot 10^{-4}$ (resp. $2.3 \cdot 10^{-5}$) is needed at 20 eV (red arrows), and $2 \cdot 10^{-4}$ (resp. $1 \cdot 10^{-5}$) at 50 eV (green arrows). An abrupt application of Eq. (1), with parameters for aluminum at 50 eV ($a = 769$, $b = 0.78$, $\Delta P = 0.1\%$), predicts a LLO $\simeq 10^{-5}$ close to the one mentioned in the MgO paper¹⁵ at 100 eV. We believe that these scalings are very general and can be found for any material and thermodynamic quantities.

The precision of a finite temperature calculation is thus tightly bound to the occupancy level of the highest band in energy involved in the calculation. An estimation of this number is desirable to calibrate the parameters of a simulation (number of bands, number of atoms) for given computer resources.

III. HOMOGENEOUS ELECTRON GAS MODEL

The electronic state occupancy being given by the Fermi-Dirac statistics, the fundamental parameter for high temperature KSDFT simulations is not the temperature itself, but rather the Fermi degeneracy defined by $\theta = k_B T / \epsilon_F$.

For a HEG, the Fermi energy ϵ_F , expressed in atomic units $e = m = \hbar = 1$ reads

$$\epsilon_F = k_B T_F = \left(\frac{2}{G} \right)^{2/3} \frac{(3\pi^2)^{2/3}}{2} n_V^{2/3}, \quad (2)$$

where $n_V = N_V / V_{at}$ is the electronic density. V_{at} is the atomic volume, N_V is the number of valence electrons, and G the degeneracy of the electronic state.

In a KSDFT approach the valence electrons are defined as electrons not belonging to the frozen core of the pseudopotential. These electrons participate to the global electronic

density and can be bound or free. Usually, for aluminum, the outermost three electrons ($3s^2 3p^1$) are counted in the valence states, which is enough up to a few eV. But if we want to go to much higher temperatures, 11 electrons ($2s^2 2p^6 3s^2 3p^1$) must be considered, leaving the very deep $1s^2$ states in the core. To reach extreme conditions, beyond 1 000 eV, an all-electron description is necessary.

The number of orbitals fulfilling a stipulated LLO α can be estimated from the HEG properties. In the following, we use the Fermi-Dirac distribution with a G degeneracy as in the ABINIT software package

$$f(\epsilon) = \frac{G}{e^{\beta(\epsilon-\mu)} + 1}, \quad (3)$$

where $\beta = 1/k_B T$, ϵ the energy and μ the chemical potential.

The energy for which the Fermi-Dirac distribution is equal to α is

$$E_\alpha^* = \theta \ln \left[\frac{G}{\alpha} - 1 \right] + \mu^*, \quad (4)$$

where we have introduced the dimensionless quantities $\mu^* = \mu / \epsilon_F$ and $E_\alpha^* = E_\alpha / \epsilon_F$. $\alpha = 10^{-2}, 10^{-3}, \dots, 10^{-6}$ is the requested last orbital occupation. The chemical potential of the HEG, obtained by comparing the number of particles at zero temperature with its expression at finite temperature⁵¹, reads

$$\mu^* = \theta I_{1/2}^{-1}[y], \quad (5)$$

where $y = \frac{2}{3}\theta^{-3/2}$. In this expression, $I_{1/2}^{-1}$ is the inverse of the Fermi integral of order 1/2. The chemical potential is equal to the Fermi energy at zero temperature, is zero for $\theta = 1$ and becomes negative for large θ .

The number of quantum states per atom is

$$\begin{aligned} N^* &= \frac{G}{2} \frac{2^{3/2}}{3\pi^2} V \epsilon^{3/2} \\ &= \frac{G}{2} \frac{2^{3/2}}{3\pi^2} V \epsilon_F^{3/2} (\epsilon / \epsilon_F)^{3/2} \\ &= N_V \epsilon^{*3/2}. \end{aligned} \quad (6)$$

The number of orbitals is thus

$$N_o = N_V / G * \epsilon^{*3/2}. \quad (7)$$

Introducing Eq. (4), we obtain the number of doubly occupied states ($G=2$) per atom and per valence electrons

$$N_o = \theta^{3/2} \left(\ln \left[\frac{2}{\alpha} - 1 \right] + I_{1/2}^{-1} \left[\frac{2}{3} \theta^{-3/2} \right] \right)^{3/2} / 2. \quad (8)$$

The total number of doubly occupied orbitals needed for a simulation of N_{at} atoms with N_V valence electrons is thus $N_{tot} = N_o N_{at} N_V$.

Using the high temperature approximation $\beta\mu \approx \ln[y]$ and dropping the 1 in the first logarithm of Eq. (8) yields the simplified expression

$$N_o^{HT} \approx \theta^{3/2} \left(\ln \left[\frac{4}{3\alpha\theta^{3/2}} \right] \right)^{3/2} / 2. \quad (9)$$

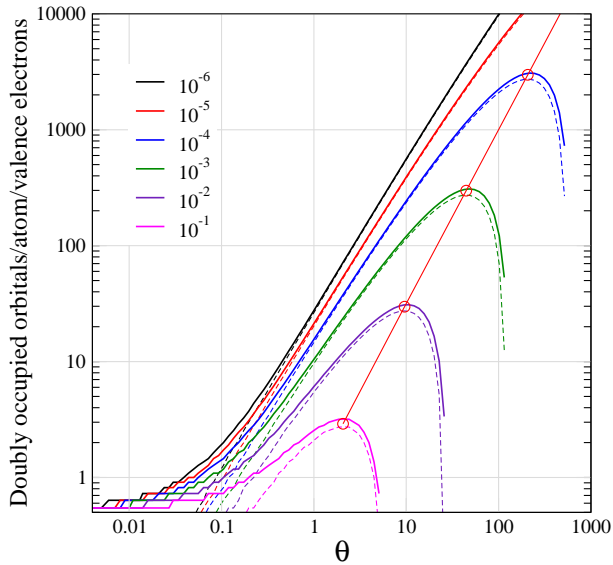


FIG. 2. (Color online) Universal curve giving the number of doubly occupied orbitals per atom and per valence electrons in the HEG model versus degeneracy θ . Colors represent the various stipulated lowest occupations LLO from 10^{-6} (top black) to 10^{-1} (bottom magenta). Solid lines: exact calculation (8) and dashed lines: high temperature approximation (9). The solid red line with red circles locates the corresponding maxima.

The latter expression predicts about 2-3% less orbitals at high temperature ($T \gtrsim T_F$) than the exact one but does not require to compute a Fermi integral. This formulation must not be used below $0.1T_F$.

The universal curve giving the number of doubly occupied orbitals per atom and per valence electrons versus reduced temperature θ is drawn in Fig. 2, for increasing LLOs from 10^{-6} (top black) to 10^{-1} (bottom magenta). The constant LLO curves are non-monotonic, but exhibit a maximum and then drop to zero. For each LLO, there is a maximum temperature θ_{\max} beyond which a bijection between the number of orbitals and temperature cannot be established. The temperature corresponding to this maximum is well approximated, by taking the temperature derivative of Eq. (9)

$$\theta_{\max} = \frac{1}{e} \left(\frac{2G}{3\alpha} \right)^{2/3}, \quad (10)$$

where $e = 2.71838$ is the usual Neper or Euler number. The maxima correspond to the maximum doubly occupied orbitals per atom

$$N_{\alpha} = \frac{1}{e^{3/2}} \left(\frac{3}{2} \right)^{3/2} \frac{2G}{3\alpha}, \quad (11)$$

that are shown by open circles in Fig. 2. These maxima are connected by the relation $N_{\alpha} = (3/2)^{3/2} \theta^{3/2}$, solid red line in Fig. 2.

In Fig. 3 we apply Eq. (8) to a system of 64 aluminum atoms with 11 valence electrons at standard density. At low temper-

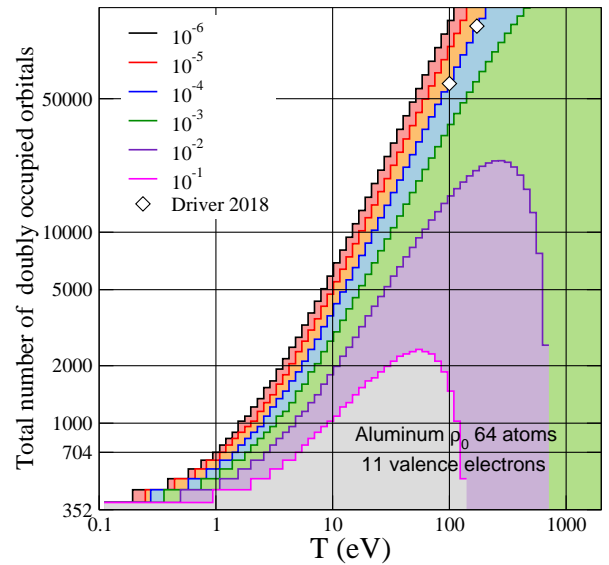


FIG. 3. (Color online) Same as Fig. 2 for a system of 64 aluminum atoms at standard density versus temperature ($N_V = 11$ valence electrons). White diamonds represent the total number of orbitals used by Driver⁵² for 8 atoms simulations at 100 and 200 eV, rescaled to 64 atoms.

ature (0.1 eV), we can see that ($64 \times 11/2 = 352$) doubly occupied orbitals are enough to satisfy any level of accuracy. At 10 eV this number grows to 1000 orbitals for a LLO of 10^{-1} and 3700 orbitals for a LLO of 10^{-4} . These numbers are rapidly growing with temperature (as $T^{3/2}$), reaching values of about 50000 orbitals at 100 eV. Lets recall that for aluminum at standard density the Fermi energy is 26.65 eV for a 11 electrons pseudo-potential. We have reported in Fig. 3 the number of orbitals used

As a test, we have added in Fig. 3 two points taken from KSDFT simulations done by Driver⁵², on aluminum at 100 and 200 eV and at standard density. For a LLO of 10^{-4} , up to 76000 bands are needed for a 64 atoms simulation at 100 eV, in agreement with the predictions of our model⁵³. To reduce the computational load, 16 and 8 atoms were used at 100 eV in the above mentioned simulations.

IV. VALIDATION

A. Comparison with occupations given by Abinit,

Fig. 4 compares the LLO predicted by the HEG model (Eq. (8), solid and dashed lines) with the same quantity obtained from an ABINIT electronic minimization (symbols), with an increasing number of orbitals at a given temperature for a four aluminum atoms system at standard density. For each minimization, the occupations are averaged over the 8^3 k-points. The agreement is good on a wide range of high temperatures. The only difference is observed at low temperature (20 eV) where the HEG formula clearly overestimates the

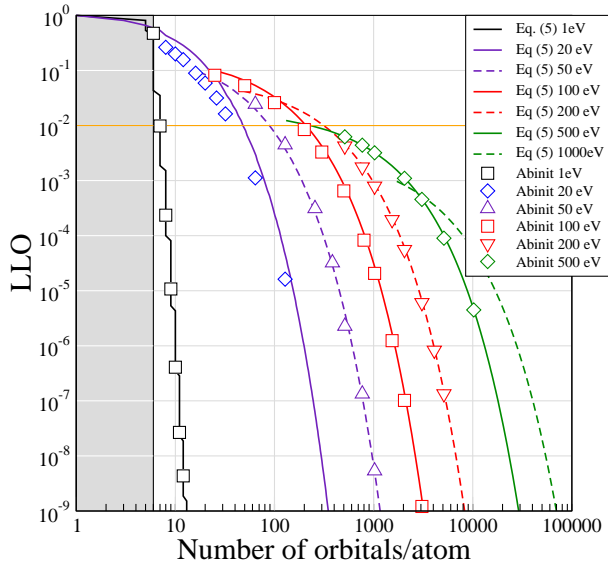


FIG. 4. (Color online) Last level occupation from ABINIT minimizations (symbols) on aluminum compared with Eq. (8) (solid and dashed lines) for different temperatures from 0.001 to 1000 eV, at standard density.

LLO obtained with ABINIT (blue diamonds).

B. Comparison with previous high temperature KSDFT simulations

The first paper to present a careful estimation of population levels, is a study of warm dense lithium³⁶ at various densities and at temperatures up to 100 kK (8.6 eV). We reported the corresponding data⁵⁴, in Fig. 5 for the various lithium densities (lines). Our prediction is shown by symbols of corresponding colors. We note that at standard density (orange line and circles) the band number is overestimated by about 35% (e.g. 110 bands instead of 80 for a stipulated occupation of 10^{-6}), but reduces to 10% at high density (4 g/cm^3 , 22 predicted bands for 20 measured in the simulation for a stipulated occupation of 10^{-6}). This is consistent with the previous ABINIT minimizations shown in Fig. 4. We interpret the depopulation of high energy states with the density, as the consequence of the modification of the chemical potential.

We have also reported in Fig. 6 the number of bands used by Luo et al.⁴⁷ (Table I of supplemental) to comply with a stipulated occupation of 10^{-6} for a simulation of 4 aluminium atoms at 2.3 g/cm^3 (blue circles in Fig. 6 (a)) and a eight silicon atoms at 2 g/cm^3 (green circles in Fig. 6 (b)). We observe in both cases a very good agreement with Eq. (8) (blue line).

Finally, we checked that the predictions of our model (Eq. 8) are consistent with the number of orbitals mentioned in various publications^{10,12,49,50,55,56} with a slight trend to overestimate the number of bands at low temperature. For instance, we obtain 192 bands for a 64 aluminum system with a $\text{LLO}=10^{-3}$ at standard density and at 1 eV instead of 180, as

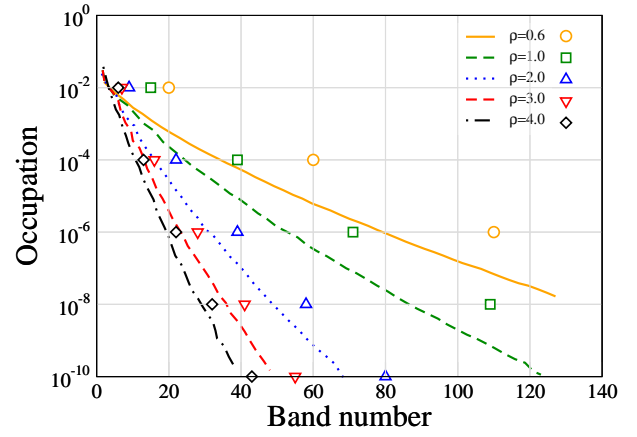


FIG. 5. (Color online) Average occupations versus band number for lithium at 8.6 eV and for various densities listed (in g/cm^3). Lines: data from Karasiev³⁶; symbols: our model.

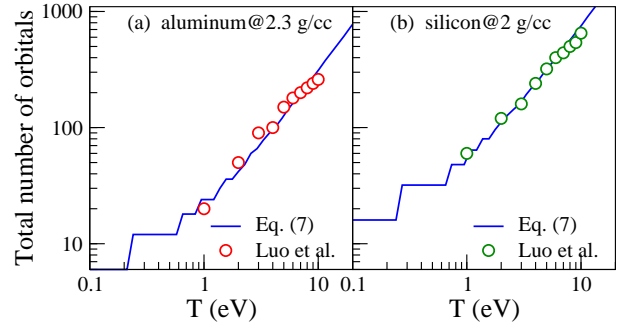


FIG. 6. (Color online) Comparison of the number of orbitals versus temperature predicted by of Eq. (8) (blue curve) with Luo et al.⁴⁷ (Table I of supplemental) for: (a) 4 aluminium atoms at 2.3 g/cm^3 (blue circles), and (b) eight silicon atoms at 2 g/cm^3 (green circles). The LLO is 10^{-6} .

published by Sjostrom⁵⁰, and to be compared to a minimum of 96 bands at zero temperature.

In conclusion of this section, the simple HEG model predicts a number of bands satisfying a stipulated precision in agreement with previous high temperature simulations. At low density and low temperature our model overestimates this number but provides a safe estimate, which can be very large, making KSDFT simulations very time consuming in some situations. This calls for models tailored to reduce this number at high temperature as we are going to show with the extended FPMD method.

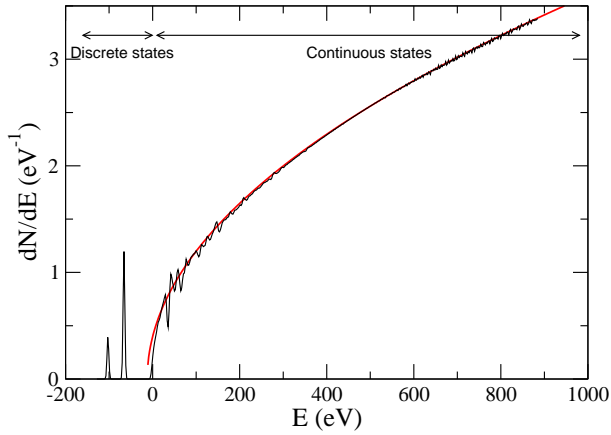


FIG. 7. (Color online) FCC Al DOS at 20 eV and standard density computed with 770 k -points. In red, the HEG density of states.

V. BYPASSING THE NUMBER OF ORBITALS CONSTRAINT

A. The extended FPMD method

In their paper Zhang *et al.*⁴⁴ suggested to use the HEG properties to simplify the description of hot dense matter. This connection, between high energy orbitals and HEG is particularly clear when we consider the density of states (DOS) of a hot system shown in Fig. 7. The DOS of aluminum at standard density and at 20 eV, computed with ABINIT and averaged over 770 k -points reveals bounded levels, at negative energies, merging with a continuum at high energy which closely follows the HEG result

$$D(\varepsilon) = \frac{\sqrt{2}\Omega}{\pi^2} \sqrt{\varepsilon - U_0}, \quad (12)$$

where Ω is the volume and U_0 a shift in the energy, to be determined.

At finite temperature, the evaluation of thermodynamic quantities (density, energy, entropy) can be broken into two parts: a discrete part accounting for N_c discrete levels and a quasi-continuous part, corresponding to densely distributed atomic states, through the DOS $g(\varepsilon)$. The energy, for example, can be written as

$$E = - \sum_{i=1}^{N_c} f(\varepsilon_i) \langle \psi_i | \nabla^2 | \psi_i \rangle + \int_{E_C}^{\infty} f(\varepsilon) g(\varepsilon) \varepsilon d\varepsilon, \quad (13)$$

where N_c is the number of considered eigenstates states ψ_i with occupation f . The occupation $f(\varepsilon_c)$ is nothing else than our previously introduced LLO. Fig. 7 suggests, to use the HEG density of states, beyond asome cutoff energy. For the electronic density, by example, we end up with the following formulation

$$n(\mathbf{r}) = 2 \sum_{i=1}^{N_c} f(\varepsilon_i) |\psi_i(\mathbf{r})|^2 - \frac{1}{\Omega} \int_{E_C}^{\infty} f(\varepsilon) D(\varepsilon) d\varepsilon \quad (14)$$

$$= n(\mathbf{r})_{KS} + n_0, \quad (15)$$

TABLE III. Comparison with Zhang's paper for hot electrons at 408 eV in a cold FCC lattice of aluminum at $\rho = 2.7 \text{ g/cm}^3$. For each quantity the first line is Zhang's results and the second line, in italic, our result.

	Reference	extended FPMD
	FT-DFT	Calc. 2
μ	-64.419	-64.512
(Ha)	-65.410	<i>-64.520</i>
E	-1 097.33	-1 098.41
(Ha)	<i>-1 097.09</i>	<i>-1 097.74</i>
-TS	-1 202.777	-1 209.604
(Ha)	<i>-1 201.236</i>	<i>-1 208.122</i>
P	4.11 10^4	4.21 10^4
(GPa)	<i>4.12 10^4</i>	<i>4.22 10^4</i>

where the constant density n_0 is given by

$$n_0 = - \frac{2\sqrt{2}}{\pi^2 \beta^{3/2}} I_{1/2}^{\text{inc}}(\eta, x_c). \quad (16)$$

$I_{1/2}^{\text{inc}}(\eta, x_c)$ is the incomplete Fermi integral of index 1/2 of argument $\eta = \beta\mu$ and lower bound $b = \varepsilon_c$, whose general definition is

$$I_{1/2}^{\text{inc}}(\eta, b) = \int_b^{\infty} \frac{x^{1/2}}{e^{x-\eta} + 1} dx. \quad (17)$$

This integral, that can be very precisely computed, is equivalent to an infinitely small LLO. Zhang *et al.*⁴⁴ have shown that a non negligible part of the precision lies between 10^{-4} and 10^{-6} LLO. It must be emphasized that N_c is now fully decoupled from the stipulated precision since the *missing* density, pressure or energy can be exactly computed.

B. Validation of implementation

We implemented the extended FPMD method into the ABINIT software package, with the projector augmented wave (PAW) method. Depending on the temperature, different atomic datas relatively to the electronic temperature were considered. From T=0 eV to T=50 eV, we used a PAW-LDA small core (11 valence electrons) pseudo-potential generated by N. A. W. Holzwarth with ATOMPAW software⁵⁷. From T=50 eV to T=500 eV, we used a PAW-GGA pseudo-potential with a smaller core, also used by K. P. Driver⁵² on his aluminum KSDFT/PIMC computations. For temperatures higher than T=500 eV, an ultrasoft all-electrons pseudo-potential generated by V. Recoules with ATOMPAW, was necessary.

For all pseudo-potentials we used a cutoff between 50 and 100 Ha, after checking, for each temperature, the convergence of the pressure. The core radius was varied from 1.6 Bohr, at low temperature, to 0.6 Bohr, at high temperature, to prevent any significant PAW spheres overlapping during molecular dynamics. For the exchange-correlation functional, we

used the local density approximation⁵⁸ up to 200 eV, and the generalized gradient approximation Perdew-Burke-Ernzerhof (PBE)⁵⁹ beyond. All simulations, from 64 to 8 atoms were performed at the Γ point.

To check our implementation, we compare in Table III the thermodynamic quantities (chemical potential μ , energy E , entropy $-TS$ and pressure P) for hot electrons at 408 eV in a cold FCC lattice of aluminum at $\rho = 2.7 \text{ g/cm}^3$ given by Zhang *et al.*⁶⁰ with our evaluation. For this particular case, we used the settings given in Zhang's paper: a cutoff of 250 Ha, the GGA-PBE exchange correlation, a cutoff radius of 0.6 Bohr, and an all-electrons PAW pseudo-potential. Our calculation is using the analytical expression (16) which is equivalent to `calc. 2` evaluation. We note an excellent agreement with all quantities, better than 0.1%. The same calculation with 11 electrons in the pseudo-potential and frozen 1s core electrons would have given 5% less pressure, signaling the onset of the ionization of the core electrons in this regime.

To test the efficiency of the method on a wide range of temperatures, we computed the pressure along the aluminum standard density isochore, from 0.1 to 2000 eV. Results are gathered in Table IV, in which the first column indicates the temperature in eV and the second one, the number of orbitals per atom stipulated by Eq. (8) satisfying a LLO of 10^{-4} . The next column (4) gives the number of orbitals per atom we used in our implementation of the extended FPMD method which is well below the previous one, and corresponds to a LLO in the vicinity of 10^{-2} . The comparison of our estimation (column 6) with Driver's results⁵² (column 5) demonstrates an excellent agreement, with an accuracy of about 1%, for a much lower computational effort, particularly beyond 200 eV, where classical KSDFT simulations are extremely time-consuming and are replaced by PIMC simulations. The maximum deviation occurs at 1 eV, reaching 1.5% and is related to the interpolation of Driver's data, computed at rounded values in K (10 000, 20 000, 50 000 and 1000 000 K).

We stress, that even well below 100 eV, the extended FPMD method is roughly one order of magnitude faster than the corresponding KSDFT calculation.

VI. CONCLUSION

We have provided a quantitative estimation of the number of orbitals needed to reach a given level of precision at any temperature for a KSDFT calculation. We have shown that, for a fixed precision, this number increases dramatically with the temperature, making extremely time-consuming KSDFT simulations of matter at standard density and below, beyond a few tens of eVs. We have then implemented the extended FPMD method in the ABINIT software package and shown how the introduction of the homogeneous electron gas density properties allows to correct poorly converged Kohn-Sham calculations with small number of orbitals, allowing to reach keVs temperatures straightforwardly.

TABLE IV. Total pressures obtained by the extended FPMD method, along the aluminum isochore ρ_0 . N_o is the prescription given by Eq. (8) for an LLO of 10^{-4} and N_o^{Ext} the number of orbitals used in the calculation. P_{Driver} values are interpolation of pressures of Driver *et al.*⁵² to the temperatures shown. The last column indicates the precision $100|P_{\text{Ext}} - P_{\text{Driver}}|/P_{\text{Driver}}$.

T eV	N_o /at Eq. (8)	N_o^{Ext} /at extended FPMD	N_{at}	P_{Ext} GPa	P_{Driver} GPa	error %
0.1	6	6	64	6.0	-	-
1	11	11	64	39.1	39.7	1.4
2	11	11	64	70.5	71.2	1.0
10	49	16	64	334.7	337.2	0.7
20	115	32	32	744.3	753.3	1.2
100	814	64	16	7681	7693	0.2
200	1 837	128	16	19 298	19400	0.5
500	5 126	256	8	59 907	59 952	0.1
1 000	10 428	256	8	129 170	130 042	0.6
2 000	19 332	256	8	264 018	266 235	0.8

ACKNOWLEDGMENTS

Vanina Recoules, Francois Soubiran and Burkhard Militzer are warmly acknowledged for stimulating discussions and for providing data and pseudo-potentials.

The data on aluminum isochore that support the findings of this study are available in the Supplemental of Driver's paper⁵², and other data are given in the Tables.

¹P. Hohenberg and W. Kohn, Phys. Rev. B **136**, 864 (1964).

²W. Kohn and L. J. Sham, Phys. Rev. A **140**, 1133 (1965).

³G. Kresse and J. Furthmüller, Computational Materials Science **6**, 15 (1996), ISSN 0927-0256, URL <http://www.sciencedirect.com/science/article/pii/S0927025696000080>.

⁴P. Giannozzi, S. Baroni, N. Bonini, M. Calandra, R. Car, C. Cavazzoni, D. Ceresoli, G. L. Chiarotti, M. Cococcioni, I. Dabo, et al., Journal of Physics: Condensed Matter **21**, 395502 (2009), URL <https://doi.org/10.1088/2F0953-8984/2F21%2F39%2F395502>.

⁵The ABINIT code is a common project of the Université Catholique de Louvain, Corning Incorporated, CEA and other contributors, (URL <http://www.abinit.org>).

⁶X. Gonze, B. Amadon, P.-M. Anglade, J.-M. Beuken, F. Bottin, P. Boulanger, F. Bruneval, D. Caliste, R. Caracas, M. Côté, et al., Computer Physics Communications **180**, 2582 (2009), ISSN 0010-4655, 40 YEARS OF CPC: A celebratory issue focused on quality software for high performance, grid and novel computing architectures, URL <http://www.sciencedirect.com/science/article/pii/S0010465509002276>.

⁷X. Gonze, B. Amadon, G. Antonius, F. Arnardi, L. Baguet, J.-M. Beuken, J. Bieder, F. Bottin, J. Bouchet, E. Bousquet, et al., Computer Physics Communications **248**, 107042 (2020), ISSN 0010-4655, URL <http://www.sciencedirect.com/science/article/pii/S0010465519303741>.

⁸N. D. Mermin, Phys. Rev. **137**, A1441 (1965), URL <https://link.aps.org/doi/10.1103/PhysRev.137.A1441>.

⁹G. Kresse and J. Hafner, Phys. Rev. B **47**, 558 (1993), URL <https://link.aps.org/doi/10.1103/PhysRevB.47.558>.

¹⁰V. Recoules, F. Lambert, A. Decoster, B. Canaud, and J. Clérouin, Phys. Rev. Lett. **102**, 075002 (2009), URL <http://link.aps.org/doi/10.1103/PhysRevLett.102.075002>.

¹¹T. Sjostrom, S. Crockett, and S. Rudin, Phys. Rev. B **94**, 144101 (2016), URL <https://link.aps.org/doi/10.1103/PhysRevB.94.144101>.

¹²S. X. Ding, Y. Hand Hu, Physics of Plasmas **24**, 062702 (2017), <https://doi.org/10.1063/1.4984780>, URL <https://doi.org/10.1063/1.4984780>.

- ¹³S. X. Hu, V. V. Karasiev, V. Recoules, P. M. Nilson, N. Brouwer, and M. Torrent, *Nature Communications* **11**, 1989 (2020), URL <https://doi.org/10.1038/s41467-020-15916-3>.
- ¹⁴M. Bethkenhagen, B. B. L. Witte, M. Schörner, G. Röpke, T. Döppner, D. Kraus, S. H. Glenzer, P. A. Sterne, and R. Redmer, *Phys. Rev. Research* **2**, 023260 (2020), URL <https://link.aps.org/doi/10.1103/PhysRevResearch.2.023260>.
- ¹⁵F. Soubiran, F. González-Cataldo, K. P. Driver, S. Zhang, and B. Militzer, *The Journal of Chemical Physics* **151**, 214104 (2019), <https://doi.org/10.1063/1.5126624>, URL <https://doi.org/10.1063/1.5126624>.
- ¹⁶W. Kohn, *Phys. Rev. Lett.* **76**, 3168 (1996), URL <https://link.aps.org/doi/10.1103/PhysRevLett.76.3168>.
- ¹⁷E. Prodan and W. Kohn, *Proceedings of the National Academy of Sciences* **102**, 11635 (2005), ISSN 0027-8424, <https://www.pnas.org/content/102/33/11635.full.pdf>, URL <https://www.pnas.org/content/102/33/11635>.
- ¹⁸E. L. Pollock and D. M. Ceperley, *Phys. Rev. B* **30**, 2555 (1984), URL <https://link.aps.org/doi/10.1103/PhysRevB.30.2555>.
- ¹⁹S. Zhang, K. P. Driver, F. Soubiran, and B. Militzer, *Phys. Rev. E* **96**, 013204 (2017), URL <https://link.aps.org/doi/10.1103/PhysRevE.96.013204>.
- ²⁰B. Militzer and K. P. Driver, *Phys. Rev. Lett.* **115**, 176403 (2015), URL <https://link.aps.org/doi/10.1103/PhysRevLett.115.176403>.
- ²¹P. Suryanarayana, P. P. Pratapa, A. Sharma, and J. E. Pask, *Computer Physics Communications* **224**, 288 (2018), ISSN 0010-4655, URL <http://www.sciencedirect.com/science/article/pii/S0010465517304022>.
- ²²Y. Cytter, E. Rabani, D. Neuhauser, and R. Baer, *Phys. Rev. B* **97**, 115207 (2018), URL <https://link.aps.org/doi/10.1103/PhysRevB.97.115207>.
- ²³A. J. White and L. A. Collins, *Phys. Rev. Lett.* **125**, 055002 (2020), URL <https://link.aps.org/doi/10.1103/PhysRevLett.125.055002>.
- ²⁴P. A. Sterne, S. B. Hansen, B. G. Wilson, and W. A. Isaacs, *High Energy Density Physics* **3**, 278 (2007).
- ²⁵C. E. Starrett and D. Saumon, *Phys. Rev. E* **93**, 063206 (2016), URL <https://link.aps.org/doi/10.1103/PhysRevE.93.063206>.
- ²⁶C. E. Starrett, *Phys. Rev. E* **96**, 013206 (2017).
- ²⁷F. Perrot and M. W. C. Dharma-Wardana, *Phys. Rev. E* **62**, 5352 (1995).
- ²⁸C. Blancard and G. Faussurier, *Phys. Rev. E* **69**, 016409 (2004).
- ²⁹G. Faussurier, C. Blancard, P. Cossé, and P. Renaudin, *Physics of Plasmas* **17**, 052707 (pages 11) (2010).
- ³⁰F. Lambert, J. Clérouin, S. Mazevet, and D. Gilles, *Contributions to Plasma Physics* **47**, 272 (2007), <https://onlinelibrary.wiley.com/doi/pdf/10.1002/ctpp.200710037>, URL <https://onlinelibrary.wiley.com/doi/abs/10.1002/ctpp.200710037>.
- ³¹F. Lambert, J. Clérouin, J.-F. Danel, L. Kazandjian, and S. Mazevet, *Properties of Hot and Dense Matter by Orbital-Free Molecular Dynamics* (World Scientific, Singapore, 2013), vol. 6 of *Recent Advances in Computational Chemistry*, pp. 165–201.
- ³²C. Ticknor, J. D. Kress, L. A. Collins, J. Clérouin, P. Arnault, and A. Decoster, *Phys. Rev. E* **93**, 063208 (2016), URL <http://link.aps.org/doi/10.1103/PhysRevE.93.063208>.
- ³³A. J. White, L. A. Collins, J. D. Kress, C. Ticknor, J. Clérouin, P. Arnault, and N. Desbiens, *Phys. Rev. E* **95**, 063202 (2017), URL <https://link.aps.org/doi/10.1103/PhysRevE.95.063202>.
- ³⁴J. Clérouin, P. Arnault, B.-J. Gréa, S. Guisset, M. Vandenboomgaerde, A. J. White, L. A. Collins, J. D. Kress, and C. Ticknor, *Phys. Rev. E* **101**, 033207 (2020), URL <https://link.aps.org/doi/10.1103/PhysRevE.101.033207>.
- ³⁵V. V. Karasiev and S. B. Trickey, *Computer Physics Communications* **183**, 2519 (2012).
- ³⁶V. V. Karasiev, T. Sjöstrom, and S. B. Trickey, *Phys. Rev. E* **86**, 056704 (2012), URL <https://link.aps.org/doi/10.1103/PhysRevE.86.056704>.
- ³⁷V. V. Karasiev, D. Chakraborty, O. A. Shukruto, and S. B. Trickey, *Phys. Rev. B* **88**, 161108 (2013), URL <https://link.aps.org/doi/10.1103/PhysRevB.88.161108>.
- ³⁸T. Sjöstrom and J. Daligault, *Phys. Rev. B* **88**, 195103 (2013), URL <http://link.aps.org/doi/10.1103/PhysRevB.88.195103>.
- ³⁹T. Sjöstrom and S. Crockett, *Phys. Rev. B* **92**, 115104 (2015), URL <https://link.aps.org/doi/10.1103/PhysRevB.92.115104>.
- ⁴⁰S. Mazevet, F. Lambert, F. Bottin, G. Zérah, and J. Clérouin, *Phys. Rev. E* **75**, 056404 (2007), URL <https://link.aps.org/doi/10.1103/PhysRevE.75.056404>.
- ⁴¹T. Sjöstrom and S. Crockett, *Phys. Rev. B* **92**, 115104 (2015), URL <https://link.aps.org/doi/10.1103/PhysRevB.92.115104>.
- ⁴²D. Sheppard, J. D. Kress, S. Crockett, L. A. Collins, and M. P. Desjarlais, *Phys. Rev. E* **90**, 063314 (2014), URL <http://link.aps.org/doi/10.1103/PhysRevE.90.063314>.
- ⁴³J. F. Danel, L. Kazandjian, and G. Zérah, *Physics of Plasmas* **19**, 122712 (2012), URL <https://doi.org/10.1063/1.4773191>.
- ⁴⁴S. Zhang, H. Wang, W. Kang, P. Zhang, and X. T. He, *Physics of Plasmas* **23**, 042707 (2016), <http://dx.doi.org/10.1063/1.4947212>, URL <http://dx.doi.org/10.1063/1.4947212>.
- ⁴⁵J. Gaffney, S. Hu, P. Arnault, A. Becker, L. Benedict, T. Boehly, P. Celliers, D. Ceperley, O. Čertík, J. Clérouin, et al., *High Energy Density Physics* **28**, 7 (2018), ISSN 1574-1818, URL <http://www.sciencedirect.com/science/article/pii/S1574181818300508>.
- ⁴⁶P. Grabowski, S. Hansen, M. Murillo, L. Stanton, F. Graziani, A. Zylstra, S. Baalrud, P. Arnault, A. Baczewski, L. Benedict, et al., *High Energy Density Physics* **37**, 100905 (2020), ISSN 1574-1818, URL <http://www.sciencedirect.com/science/article/pii/S1574181820301282>.
- ⁴⁷K. Luo, V. V. Karasiev, and S. B. Trickey, *Phys. Rev. B* **101**, 075116 (2020), URL <https://link.aps.org/doi/10.1103/PhysRevB.101.075116>.
- ⁴⁸We count two electrons for one electronic state ($G=2$), also referred as orbital.
- ⁴⁹T. Sjöstrom and J. Daligault, *Phys. Rev. Lett.* **113**, 155006 (2014), URL <http://link.aps.org/doi/10.1103/PhysRevLett.113.155006>.
- ⁵⁰T. Sjöstrom and J. Daligault, *Phys. Rev. E* **92**, 063304 (2015), URL <https://link.aps.org/doi/10.1103/PhysRevE.92.063304>.
- ⁵¹G. Chabrier and A. Y. Potekhin, *Phys. Rev. E* **58**, 4941 (1998), URL <https://link.aps.org/doi/10.1103/PhysRevE.58.4941>.
- ⁵²K. P. Driver, F. Soubiran, and B. Militzer, *Phys. Rev. E* **97**, 063207 (2018), URL <https://link.aps.org/doi/10.1103/PhysRevE.97.063207>. Private communication.
- ⁵⁴Data are reported in Fig. 8 of the paper: V. Karasiev, T. Sjöstrom, and S. B. Trickey, *Phys. Rev. E* **86**, 056704 (2012).
- ⁵⁵F. Lambert, V. Recoules, A. Decoster, J. Clérouin, and M. Desjarlais, *Physics of Plasmas* **18**, 056306 (2011), URL <https://doi.org/10.1063/1.3574902>.
- ⁵⁶T. Sjöstrom and J. Daligault, *Phys. Rev. B* **88**, 195103 (2013), URL <https://link.aps.org/doi/10.1103/PhysRevB.88.195103>.
- ⁵⁷N. Holzwarth, A. Tackett, and G. Matthews, *Computer Physics Communications* **135**, 329 (2001), ISSN 0010-4655, URL <http://www.sciencedirect.com/science/article/pii/S0010465500002447>.
- ⁵⁸D. M. Ceperley and B. J. Alder, *Phys. Rev. Lett.* **45**, 566 (1980).
- ⁵⁹J. P. Perdew, K. Burke, and M. Ernzerhof, *Phys. Rev. Lett.* **77**, 3865 (1996), URL <https://link.aps.org/doi/10.1103/PhysRevLett.77.3865>.
- ⁶⁰Data are reported in Table I of the paper: S. Zhang, H. Wang, W. Khang, P. Zhang, and X. T. He, *Physics of Plasmas* **23**, 042707 (2016).